Ultrafast pump-probe spectroscopy of linear molecular aggregates

Heijs, Dirk-Jan; Dijkstra, Arend G.; Knoester, Jasper

Published in:
Chemical Physics

DOI:
10.1016/j.chemphys.2007.06.050

Publication date:
2007

Available online at www.sciencedirect.com
ScienceDirect
Chemical Physics 341 (2007) 230–239
Chemical Physics
www.elsevier.com/locate/chemphys

Ultrafast pump-probe spectroscopy of linear molecular aggregates: Effects of exciton coherence and thermal dephasing

Dirk-Jan Heijs, Arend G. Dijkstra, Jasper Knoester *

Center for Theoretical Physics and Zernike Institute for Advanced Materials, University of Groningen, Nijenborgh 4, 9747 AG Groningen, The Netherlands

Received 13 April 2007; accepted 20 June 2007
Available online 14 July 2007

Abstract

We model the pump-probe spectrum of linear molecular aggregates measured by using ultrafast laser pulses. We analyze in particular the effects of coherences between exciton states created by the pump pulse and show that these give rise to a small induced-absorption peak that is red-shifted relative to the main one-exciton bleaching peak. The new coherent peak survives common values of the static disorder. With increasing pump-probe delay time, its amplitude oscillates and decays with a rate that is inversely proportional to the width of the absorption band. We also consider coupling to vibrations and show that with increasing temperature the frequency separation between the main bleaching and induced-absorption peaks increases and provides a measure for the exciton coherence size imposed by scattering on the vibrations.

Keywords: J-aggregates; Frenkel excitons; Pump-probe spectroscopy; Coherent effects

1. Introduction

The remarkable optical properties of molecular J-aggregates, caused by Frenkel excitons that are coherently delocalized over many molecules, have attracted considerable attention for more than 70 years now [1–3]. Nonlinear optical techniques, such as photon echoes and pump-probe (transient absorption) spectroscopy have enormously enhanced our knowledge about the exciton dynamics, the role of static disorder, and the properties of multi-exciton states. In the latter, two or more excitation quanta are shared by the molecules in one coherence domain. An experiment that has drawn particular attention during the past 15 years, is the pump-probe spectrum [4–18]. Typically, this spectrum reveals a dispersive line shape, characterized by a negative peak, due to bleaching and stimulated emission of the one-exciton states, and a blue-shifted positive (induced-absorption) peak, which is caused by the probe pulse inducing transitions from the one-exciton states created by the pump pulse to the two-exciton manifold. It has been shown that at low temperatures the detuning between the induced-absorption and bleaching peaks can be used to experimentally determine the exciton delocalization size imposed by static disorder [16]. It has also been suggested that at elevated temperatures the same detuning rather measures the exciton coherence size imposed by scattering on vibrations [15].

While the experiments as well as theory have initially focused on linear molecular aggregates, where Frenkel excitons can be viewed to a good approximation as fermions [5,19,20], other geometries have been considered as well, in particular circular and cylindrical molecular aggregates [13–18]. This was stimulated by the discovery that certain antenna complexes in natural photosynthetic systems as well as aggregates of amphiphilic cyanine dyes have such geometries [21–25]. The dispersive line shape of the pump-probe spectrum is maintained for such molecular assemblies as well.

In the analysis of the above pump-probe experiments one mostly uses the picture of two consecutive linear

* Corresponding author. Tel.: +31 503634369; fax: +31 503634950.
E-mail address: J.Knoester@rug.nl (J. Knoester).

0301-0104/$ - see front matter © 2007 Elsevier B.V. All rights reserved.
doi:10.1016/j.chemphys.2007.06.050

absorption experiments. The pump pulse excites a one-exciton population, while the probe pulse after some delay time interrogates the thus prepared system in a second absorption experiment. This view neglects the contributions resulting from coherences between two different one-exciton states created by the pump pulse. For two-color experiments, where the pump-probe delay time typically is long compared to the lifetime of the coherences, this may be expected to be a good approximation. Indeed, neglecting coherences gives excellent fits to experiment [6]. However, ultrafast pump-probe spectra, measured with femtosecond pulses at low temperatures, should hold signatures of coherent contributions. Since no systematic theoretical analysis has been conducted to uncover the special features arising from coherences, it currently is not clear what to look for in the spectra.

In this paper, we theoretically analyze the pump-probe spectrum of linear J-aggregates for ultrashort laser pulses. We consider two different aspects that have not received systematic attention before, namely the effects of exciton–exciton coherences and the effects of thermal dephasing on this spectrum. After setting up the general formalism, we first turn to the effects of the coherences, focusing on low temperatures, where these effects are strongest. We show that for zero pump-probe delay time these coherences result in a small positive feature that is red-shifted compared to the one-exciton bleaching peak. This new feature survives disorder and can be associated with the coherence between the lowest and third excited state of an exciton delocalization segment. According to our estimates, it should be possible to observe this feature in experiment. The new peak undergoes oscillations between positive and negative intensity (reflecting its coherent nature) and reduces in amplitude due to inhomogeneous dephasing processes. As a consequence, both the oscillations and the relaxation of the coherent peak occur at a time of the order of the inverse J-band width. After this zero-temperature analysis, we address the temperature dependence of the spectrum. We do this by calculating, from microscopic principles, the vibration-induced dephasing rates of the various excitonic transitions that contribute to the pump-probe spectrum. We use a one-phonon scattering model that recently has been shown to accurately describe the exciton dynamics of J-aggregates [26,27] and demonstrate that with increasing temperature the frequency separation between the positive and negative peaks in the main dispersive line shape provides a measure for the exciton coherence size imposed by scattering on the vibrations.

This paper is organized as follows. In Section 2, we describe the model. The calculation of the pump-probe signal is briefly addressed in the Section 3. In Section 4, we consider the low-temperature spectrum, focusing on coherent effects, while in Section 5, we present results for the change of the spectral shape for elevated temperatures. Finally, in Section 6 we conclude. The Appendix contains some details concerning the exciton–phonon scattering rates.

2. Model

We consider a linear molecular aggregate of N two-level molecules, labeled $n = 1, 2, \ldots, N$. The transition energy of molecule n is denoted ε_n; in order to model static disorder, the ε_n are taken independently from a Gaussian distribution with mean $\bar{\varepsilon}$ and standard deviation σ. Between the molecules, intermolecular excitation transfer interactions exist. In this paper we will restrict ourselves to nearest-neighbor interactions $-J$, with J positive (appropriate for J-aggregates). The details of this model can be found in many papers (see Ref. [3] for an overview).

It is well known that all multi-exciton states in this model can be found by diagonalizing the $N \times N$ tridiagonal matrix with the ε_n on its diagonal and $-J$ on its two side-diagonals. Let us denote the kth eigenvalue of this matrix E_k and the nth component of the corresponding eigenvector φ_{kn}. For our purpose, the relevant eigenstates are the ground state $|g\rangle$ (no excitations in the system), the one-exciton states $|k\rangle = \sum_{n=1}^{N} \varphi_{kn}|n\rangle$ (with $|n\rangle$ denoting the state with molecule n excited and all other molecules in the ground state), and the two-exciton states $|K\rangle = \sum_{n>m}^{N} \varphi_{Knm}|nm\rangle$ (with $|nm\rangle$ denoting the state with molecules n and m excited and all other molecules in the ground state). Due to the fermionic nature of the excitons in our model, the two-exciton may be labeled by the two one-exciton modes that have been excited, i.e., $K = (k_1, k_2)$ ($k_1 \neq k_2$) and [19,5,20]

$$\varphi_{Knm} = \varphi_{k_1 n}\varphi_{k_2 m} - \varphi_{k_1 m}\varphi_{k_2 n}. \tag{1}$$

Relative to the ground state, the energies of the one- and two-exciton states take the values E_k and $E_K = E_{k_1} + E_{k_2}$, respectively.

The transition dipoles between the ground state and the one-exciton states read

$$\mu_{kg} = \sum_{n=1}^{N} \varphi_{kn}, \tag{2}$$

while the dipole from the one-exciton state $|k\rangle$ to the two-exciton $|K\rangle$ reads

$$\mu_{Kk} = \sum_{n>m}^{N} \varphi_{Knm}(\varphi_{kn} + \varphi_{km}). \tag{3}$$

Here, we have assumed that all molecular dipoles are equal in magnitude as well as direction and we have set their magnitude equal to unity.

For future reference, it is useful to reiterate the well-known results for the eigenenergies, eigenvectors, and transition dipoles in the special case of homogeneous aggregates ($\sigma = 0$). We then have ($k = 1, 2, \ldots, N$)

$$E_k = \bar{\varepsilon} - 2J\cos\frac{\pi k}{N+1} \tag{4}$$

and

$$\varphi_{kn} = \sqrt{\frac{2}{N+1}}\sin\frac{\pi k n}{N+1}. \tag{5}$$

Expressions for the resulting transition dipoles can be found in Ref. [28]. Only one-exciton states with $k = \text{odd}$ are dipole allowed from the ground state. Almost all oscillator strength of the one-exciton band is collected in the $k = 1$ state, $\mu^2_{k=1,g} = 0.81N$, while the next largest transition is an order of magnitude weaker: $\mu^2_{k=3,g} = 0.09N$ ($N \gg 1$ assumed). Transitions from the one-exciton manifold to the two-exciton band depend on the starting state k. For $k = 1$ and $k = 3$ the dipoles and energies of the dominant transitions are given in Table 1.

To end this section, we describe the interaction between the excitons and harmonic vibrations. We will assume an onsite one-phonon interaction, resulting from the first-order variation of the site energies ε_n in powers of the vibration-induced displacements of atoms in the environment of the molecule. The corresponding interaction reads

$$H_{\text{ex–ph}} = \sum_n V_{nq}(a_q + a_q^\dagger) b_n^\dagger b_n, \tag{6}$$

with $b_n^\dagger$ (b_n) the Pauli creation (annihilation) operator for an electronic excitation on molecule n and $a_q^\dagger$ (a_q) the Bose creation (annihilation) operator for a phonon in mode q. For a disordered host, we may consider the coupling constants stochastic quantities, with $\langle V_{nq}\rangle = 0$ and $\langle V_{nq} V_{mq}\rangle = \delta_{nm}|V_q|^2$.

Obviously, the interaction Eq. (6) conserves the number of excitons and gives rise to scattering within the one- and two-exciton bands. The rates which describe these scattering processes may be calculated using Fermi's golden rule. In the Appendix, we give expressions for the various population and phase relaxation rates needed to calculate the pump-probe signal described in the next section. A quantity that plays an important role in these expressions is the one-phonon spectral density

$$\mathscr{F}(\omega) \equiv 2\pi \sum_q |V_q|^2 \delta(\omega - \omega_q), \tag{7}$$

where ω_q denotes the energy of a phonon in mode q. Like most authors, we will assume a simple form for $\mathscr{F}(\omega)$. In particular, the results presented in Section 5 were obtained using

$$\mathscr{F}(\omega) = W_0 \left(\frac{\omega}{J}\right)^3, \tag{8}$$

which models scattering on three-dimensional acoustic phonons (in the aggregate's host medium) with a Debye density of states. The overall scattering rate W_0 is a free parameter in the theory. It has been shown recently that this spectral density gives an accurate description of the exciton dynamics in linear J-aggregates [26,27].

3. Pump-probe signal

In this section, we present the general expressions for the pump-probe signal. We will assume that the applied pump and probe pulses are short compared to the inverse exciton band width, $(4J)^{-1}$, implying that all exciton transitions are excited proportional to their oscillator strength and independent of their energy. We will furthermore assume that the pump pulse interacts with the system first, i.e., we assume that the pump-probe delay τ is large compared to the pulse duration. It may be short compared to the timescale of the exciton dynamics, however.

The frequency (ω) resolved pump-probe signal, defined as the difference absorption spectrum of the probe pulse with and without pump pulse (to lowest order in the pulse intensities) may be calculated through standard techniques, employing double-sided Feyman diagrams [29]. For our purposes, it is useful to separate the total signal into an incoherent part, deriving from those contributions where the system is in a one-exciton population $|k\rangle\langle k|$ during the waiting time between both pulses, and a coherent part, where the system is in a coherence $|k\rangle\langle k'|$ ($k \neq k'$) during this time:

$$S^{\text{PP}}(\tau;\omega) \equiv S^{\text{PP}}_{\text{pop}}(\tau;\omega) + S^{\text{PP}}_{\text{coh}}(\tau;\omega). \tag{9}$$

For the incoherent part of the signal, calculation yields

$$S^{\text{PP}}_{\text{pop}}(\tau;\omega) = -\frac{1}{\pi}\sum_{k'}\left\{\mu^2_{k'g}\frac{\Gamma_{k'g}}{(\omega_{k'g}-\omega)^2+\Gamma^2_{k'g}} + \sum_{k''}\mu^2_{k''g}\frac{\Gamma_{k''g}}{(\omega_{k''g}-\omega)^2+\Gamma^2_{k''g}} - \sum_K \mu^2_{Kk'}\frac{\Gamma_{Kk'}}{(\omega_{Kk'}-\omega)^2+\Gamma^2_{Kk'}}\right\}\sum_k \left[\mathrm{e}^{\tilde{W}\tau}\right]_{k'k}\mu^2_{kg}, \tag{10}$$

where the first term arises from stimulated emission, the second from bleaching, and the third from induced absorption. Furthermore, we introduced the notation $\omega_{pq} = E_p - E_q$ for arbitrary states p and q, Γ_{pq} for the homoge-

Table 1
Dipole moments and energies of the dominant transitions from the one-exciton states $|k = 1\rangle$ and $|k = 3\rangle$ to states $|K\rangle = |(k_1, k_2)\rangle$ in the two-exciton manifold for long homogeneous chains of N molecules

K	μ_{K1}	μ_{K3}	$E_K - E_1$	$E_K - E_3$	Intensity
(1,2)	$1.13\sqrt{N}$	$0.225\sqrt{N}$	E_2	$E_1 + E_2 - E_3$	$0.068N^2$
(2,3)	$0.375\sqrt{N}$	$-0.9\sqrt{N}$	$E_2 + E_3 - E_1$	E_2	$-0.045N^2$
(1,4)	$0.225\sqrt{N}$	$0.563\sqrt{N}$	E_4	$E_1 + E_4 - E_3$	$0.034N^2$
(3,4)	$0.263\sqrt{N}$	$0.225\sqrt{N}$	$E_3 + E_4 - E_1$	E_4	$0.016N^2$

The last column gives the product $\mu_{1g}\mu_{3g}\mu_{K1}\mu_{K3}$, which equals the intensity of the coherent induced-absorption peaks occurring at $E_K - E_1$ and $E_K - E_3$, deriving from processes in which the system has been brought in the coherence $|1\rangle\langle 3|$ or $|3\rangle\langle 1|$ by the pump pulse (see Eq. (11)). These peaks and the two stimulated emission contributions at E_1 and E_3 explain all the features in the coherent part of the spectrum observed in Fig. 1b.

neous dephasing rate of the coherence between these two states, and the $N \times N$ relaxation matrix $\tilde{W}$ which governs the evolution of one-exciton populations P_k during the waiting time τ (resulting from redistribution within the one-exciton band as well as radiative decay to the ground state). Expressions for the various Γ_{pq} and the matrix elements of $\tilde{W}$, assuming that scattering on host vibrations is the source of intraband relaxation, are given in the Appendix.

For the coherent part of the signal, calculation yields

$$S_{\mathrm{coh}}^{\mathrm{PP}}(\tau;\omega) = -\frac{1}{\pi}\sum_{k,k'}{}^{*}\left\{\mu_{k'g}\mu_{kg}\frac{\Gamma_{k'g}}{(\omega_{k'g}-\omega)^2+\Gamma_{k'g}^2} - \sum_{K}\mu_{Kk'}\mu_{Kk}\frac{\Gamma_{Kk'}}{(\omega_{Kk'}-\omega)^2+\Gamma_{Kk'}^2}\right\} \times \left[\mathrm{e}^{-\Gamma_{kk'}\tau}\cos\omega_{kk'}\tau\right]\mu_{kg}\mu_{k'g}, \quad (11)$$

where the first term derives from stimulated emission and the second from induced absorption. There is no coherent bleaching contribution. The asterisk on the summation excludes the term with $k = k'$.

The incoherent signal Eq. (10) may simply be interpreted as the linear absorption spectrum of the system with initial populations $P_{k'}(\tau) = \sum_k [\mathrm{e}^{\tilde{W}\tau}]_{k'k}\mu_{kg}^2$. It depends on τ owing to the population redistribution and decay to the ground state following the pump pulse. The τ dependence of the coherent part Eq. (11) of the signal is richer, as its peaks in general will oscillate due to the (damped) quantum beats with frequencies $\omega_{kk'}$. In contrast to the incoherent part, the coherent part of the spectrum will also suffer from inhomogeneous dephasing, arising from the simultaneous occurrence of a variety of frequencies $\omega_{kk'}$ in case the system is inhomogeneous (a disorder average of the signals in Eqs. (10) and (11) is then implied). We will encounter this in Section 4.2.

4. Results: effects of coherences

In this section, we consider the pump-probe spectrum at low temperatures, focusing on the effect of the coherent contributions. We will assume that the temperature is low enough to neglect the homogeneous line widths of the exciton transitions compared to their inhomogeneous broadening. Thus, all Lorentzian factors in Eqs. (10) and (11) are replaced by Dirac delta-functions at the corresponding transition energy.

4.1. Homogeneous aggregates

Before turning to the general case of disorder, it is useful to consider the incoherent and coherent contributions for the homogeneous case, where $\sigma = 0$. Strictly speaking, the neglect of the homogeneous linewidth is then not justified anymore, but for purpose of illustration it still is useful to consider this case. Owing to the distribution of oscillator strength for the homogeneous chain (see Section 2), at $\tau = 0$ the incoherent contribution is dominated by the term with $k' = 1$. This gives rise to a dominant bleaching and stimulated emission peak at $E_{k=1}$, which is the lowest-energy resonance that occurs in the incoherent spectrum, and a dominant induced-absorption contribution at the transition between $k' = 1$ and $K = (1,2)$. The energy of the latter transition is $E_{k=2}$, which is blue-shifted by an amount $3\pi^2 J/N^2$ ($N \gg 1$) relative to the bleaching peak.

Together these two dominant contributions are responsible for the overall dispersive line shape of the pump-probe spectrum mentioned in Section 1. This main part is clearly visible in the top panel of Fig. 1, where the total spectrum (incoherent as well as coherent contributions) is plotted. Several other, smaller peaks can be discerned, some of which derive from weaker incoherent contributions, while others derive from coherent contributions. The latter are plotted separately in the bottom panel of Fig. 1 (note the difference in vertical scale). All peaks observed in this panel may be understood from the dominant dipoles to the two-exciton manifold involving the $|1\rangle\langle 3|$ and $|3\rangle\langle 1|$ coherences as the system's state created by the pump pulse (cf. Eq. (11) and Table 1). We observe that the coherent contributions slightly enhance the dispersive shape at $E_{k=1}$ and $E_{k=2}$. The most interesting coherent contribution, however, is the small positive peak red-shifted compared to the main bleaching peak and indicated by the arrow ($\omega_{\max}$). It has an intensity that is about 7–8% of the one in the main induced-absorption peak in the total

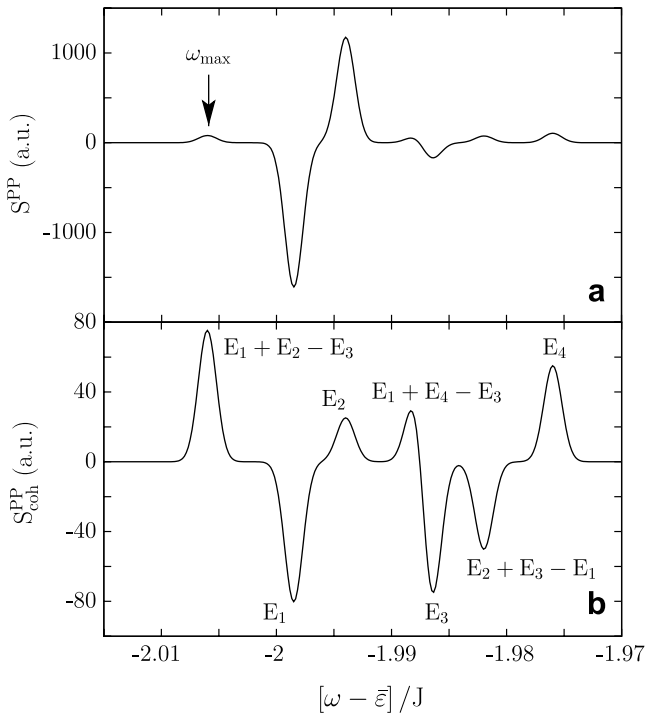

Fig. 1. Total (a) and coherent part only (b) of the pump-probe spectrum at delay $\tau = 0$ for linear molecular J-aggregates of $N = 80$ molecules without disorder ($\sigma = 0$). For purpose of presentation, all peaks have been given a finite (equal) width. In the bottom panel, the energies of the peaks are indicated.

spectrum and a resonance energy given by $E_{k=1} + E_{k=2} - E_{k=3}$, i.e., $4\pi^2 J/N^2$ lower than $E_{k=1}$. The interest in this new induced-absorption peak lies in the fact that it occurs on the low-energy side of the main bleaching peak, i.e., outside the two-exciton band and away from any other transition arising from incoherent contributions of higher lying band states. This circumstance enhances the possibility to actually observe this feature. Due the fact that the all coherent contributions are dominated by the $|1\rangle\langle 3|$ and $|3\rangle\langle 1|$ coherences, the entire coherent part of the spectrum oscillates in amplitude (and sign) with frequency $\omega_{31} \approx 8\pi^2 J/N^2$ as a function of τ. Superimposed on this oscillation is an overall decay with the homogeneous dephasing rate Γ_{13} (cf. Eq. (11)).

4.2. Disordered aggregates

In order to better assess whether the red-shifted induced-absorption peak could indeed be observed in experiment, it is important to take into account the effects of disorder. We have studied these effects by Monte Carlo averaging the incoherent and coherent signal over random disorder realizations of the site energies. Fig. 2 displays the $\tau = 0$ spectrum simulated for aggregates of $N = 80$ molecules with four different values for σ. The disorder strengths used are relevant to J-aggregates under common experimental conditions. The solid line gives the total spectrum while the dashed line only presents the coherent contributions. We observe that all spectra display the same main dispersive character as in the homogeneous case, caused by bleaching and stimulated emission of the optically dominant one-exciton band-edge states (negative peak) and induced absorption from those states to the bottom of the two-exciton band (positive). This basic shape is well known and has been analyzed by various authors (see, e.g., Ref. [16]).

The separation between the bleaching and induced-absorption maxima grows with increasing disorder, reflecting the diminishing delocalization size of the excitons. The spectral structure observed in particular for the smaller disorder strengths at the high-energy side of the induced-absorption peaks, is caused by finite size effects (i.e., N is not sufficiently large compared to the exciton delocalization size N_{del}). The transitions that are mainly responsible for the induced-absorption peak, are those between the lowest one-exciton state on a localization segment and the two-exciton state resulting from simultaneously occupying the lowest and the next higher exciton states that occur on this segment. Such doublets of excited states often occur, reflecting a hidden level structure at the lower exciton band edge (see Fig. 3) [30].

Interestingly, it is clear from Fig. 2 that, indeed, the red-shifted coherent feature survives disorder. For growing disorder strength, it decreases compared to the main dispersive lineshape, because both features broaden and thus obtain a growing overlap. As a result an increasing part of the positive coherent peak is canceled by the negative (mainly incoherent) bleaching peak. Nevertheless, it seems

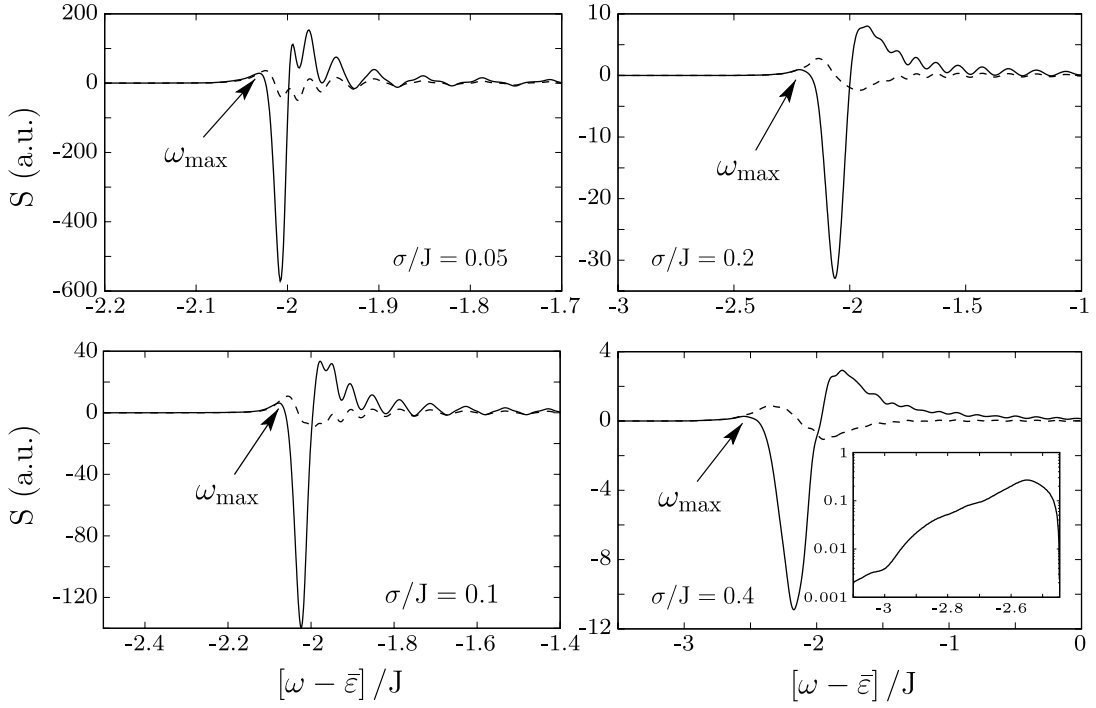

Fig. 2. The $\tau = 0$ pump-probe spectra of a linear chain of $N = 80$ molecules with disorder strengths $\sigma/J = 0.05$, 0.1, 0.2, and 0.4. The full spectrum is indicated by a solid line, the coherent part of the signal is indicated by a dashed line. The oscillatory behavior on the blue side of the main peak is caused by finite size effects. The lower right panel contains an inset which shows the frequency dependence of the red-shifted peak on a logarithmic scale. The horizontal and vertical scales of the four panels are different.

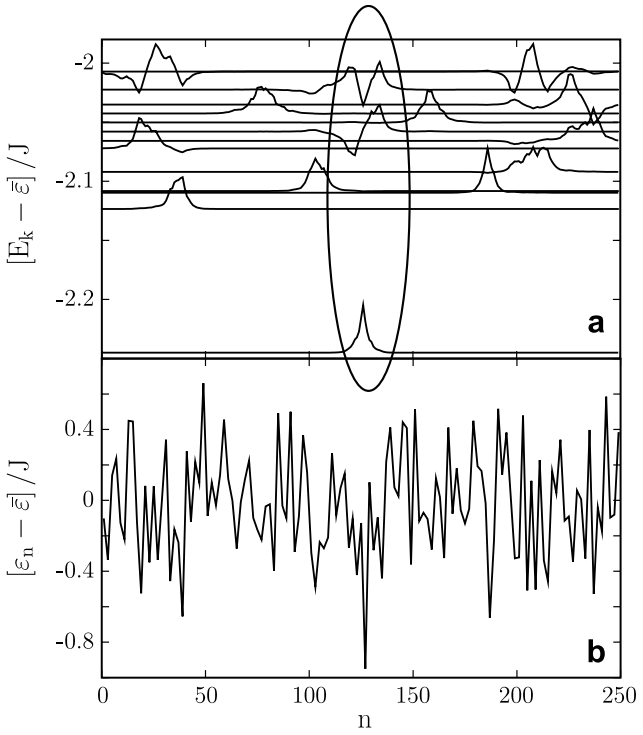

Fig. 3. (a) Wave function amplitudes as a function of position for the lowest 15 exciton states of a particular disorder realization of an inhomogeneous aggregate with $N = 250$ and $\sigma = J/4$. Indicated are the $k = 1$, $k = 2$, and $k = 3$ resembling wave functions on one particular localization segment. (b) Site energies ε_n for the above disorder realization.

that for disorder strengths relevant to experiment (e.g., $\sigma/J \approx 0.1$ for PIC (pseudo-isocyanine) aggregates [27]), the coherent induced absorption still should be observable.

It turns out that, similar to the homogeneous case, the origin of the red-shifted induced absorption can be found in three states, namely the three lowest exciton states associated with one localization segment. A typical example is seen in Fig. 3, where in the upper panel we plot the 15 lowest-energy exciton wave functions (off-set by their energy) corresponding to the disorder realization given in the lowest panel, randomly generated for $\sigma/J = 0.25$. The three states on the localization segment around the middle of the chain clearly form a triplet, which resemble the $k = 1$, $k = 2$, and $k = 3$ exciton states of the homogeneous chain, except that they are not spread over the entire chain, but rather over the localization segment only. The red-shifted coherent induced-absorption peak can be associated with processes in which the pump pulse excites a coherence between the first and third excited states on such segments, while the probe pulse further excites this to a population of the two-exciton state in which both the first and the second excited state are occupied. This is the first spectroscopic technique in which such triplets of localized states are probed. The disorder realization in the lowest panel clearly indicates that around the chain's center a negative fluctuation in the site energies exists, giving rise to a potential well that forms the localization segment. We have found that not in all cases the three states contributing to the red-shifted peak have such a clear $k = 1$, $k = 2$, and $k = 3$ nature as seen here. Often, the lowest doublet of states can clearly be recognized as $k = 1$ and $k = 2$ states on one segment, while the higher participating state is centered at the same segment, but may extend outside of it.

To end this section, we present in Fig. 4 the τ dependence of the pump-probe signal for $\sigma/J = 0.05$, 0.1, 0.2, and 0.4 at the positions $\omega_{\max}$ (indicated in Fig. 2) where the red-shifted feature reaches its maximum. It should be stressed that, as before, we neglected the homogeneous dephasing rates as well as the population relaxation rates, assuming that the spectrum and its time-dependence are dominated by inhomogeneous effects (accurate at low temperature). The signal is plotted as a function of $\Delta\tau$, where Δ is the zero-temperature full width at half maximum of the absorption band calculated for each disorder strength. As Δ increases with σ (according to $\sigma^{4/3}$) [31–33], the time scale decreases with increasing disorder.

It is clearly seen from the figure that the signal decays on a time scale $\sim 1/\Delta$. This may easily be understood as follows: as we neglected dynamics caused by scattering, the time-dependence results from the beating of the various factors $\cos(\omega_{kk'}\tau)$ in Eq. (11) associated mainly with the inhomogeneous distribution of $k = 1$ and $k' = 3$ like states on localization segments in the disordered ensemble. As the energy differences between exciton states on one segment exhibit fluctuations similar in size to the total absorption band width (which reflects the fluctuation in energy of the $k = 1$ like states) [30], indeed one expects an overall decay on a timescale similar to free induction decay, i.e., $\sim 1/\Delta$. In addition to this decay, a beating of the signal occurs on the same time scale, which reflects the fact that an average difference frequency $\omega_{kk'}$ of the order of the J-band width is relevant to the signal. The finer quantum beats visible for $\sigma/J = 0.05$ and 0.1 derive from finite size effects. Finally, we notice that for long delay times the signal does not decay to zero, but rather reaches an overall

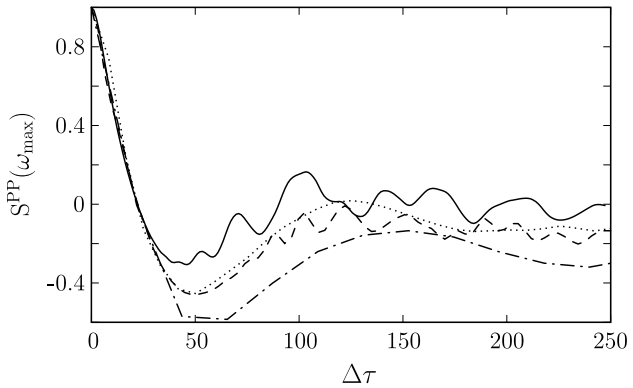

Fig. 4. The delay time dependence of the pump-probe signal, S^{PP}, for a linear chain with $N = 80$ at the position $\omega_{\max}$ of the maximum value of the red-shifted peak at $\tau = 0$ for disorder values $\sigma/J = 0.05$ (solid), 0.1 (dashed), 0.2 (dotted), and 0.4 (dash dotted). For each disorder value, the time is scaled with the corresponding zero-temperature width Δ of the J-band.

negative value, because the red wing of the (constant) negative bleaching peak then dominates the signal at $\omega_{\max}$.

5. Results: effects of thermal dephasing

In this section, we consider the effects of exciton–phonon scattering and the resulting temperature dependence of the pump-probe spectrum. In these calculations, we will neglect the coherent contributions to the spectrum. As we have seen, at $T = 0$ these contributions already are rather small and with increasing temperature they will only get weaker due to growing dephasing rates $\Gamma_{kk'}$. Moreover, we will mainly be interested in the main dispersive feature of the spectrum, which is completely dominated by incoherent contributions. We will only present results for small delay time τ, where population relaxation may be neglected, i.e., we effectively set $\tau = 0$. Finally, we will set $\sigma = 0$, thus assuming that the spectrum is dominated by thermal linewidths and not by disorder. All these restrictions also help to keep the computation time within reasonable bounds.

The main complication with respect to the previous section, is that we explicitly include the homogeneous linewidths Γ_{kg} and Γ_{Kk} of all the ground state to one-exciton and one- to two-exciton transitions needed to calculate the spectrum at finite temperature. As these linewidths are different for each pair of levels, this involves extensive calculations. In particular the calculation of the Γ_{Kk} requires the evaluation of all scattering rates within the two-exciton band (see Eq. (18) with (15b)), which causes the computation time to scale according to N^6. As a consequence, we have only considered rather short chains, with $N = 40$ and $N = 60$. We have used the expressions given in the Appendix to calculate the dephasing rates, using the spectral density Eq. (8).

Fig. 5 displays the resulting spectra for four different temperatures, using $W_0 = 25J$ as overall scattering rate. This value is typical for J-aggregates of PIC; using the value of $J = 600\ \mathrm{cm}^{-1}$ appropriate for these aggregates, the four temperatures considered correspond to 100 K, 150 K, 200 K, and 250 K, respectively. As we observe, at the lowest temperature the spectrum has its typical asymmetric dispersive lineshape, explained in Section 4.1 already. With increasing temperature, the spectrum becomes more symmetric, with the central bleaching peak being surrounded by small induced-absorption contributions. This happens because the Γ_{Kk} are much larger than the Γ_{kg}, mainly due to the fact that the density of states in the two-exciton band is much larger (by a factor of the order N) than the one in the two-exciton band, giving rise to many more scattering possibilities.

We also observe that the energy difference δ between the position where the bleaching peak has its maximum intensity and the maximum of the blue-shifted induced-absorption maximum increases with T. In the case of homogeneous aggregates at $T = 0$, we have

$$\delta(T=0) = [E_{K=(1,2)} - E_{k=1}] - E_{k=1} \approx 3\pi^2 J/N^2, \tag{12}$$

where we used Eq. (4) with $N \gg 1$. This expression, with N replaced by the exciton delocalization length, N_{del}, has been used by several authors to extract N_{del} from experiment [11–13]. The justification for this lies in the hidden level

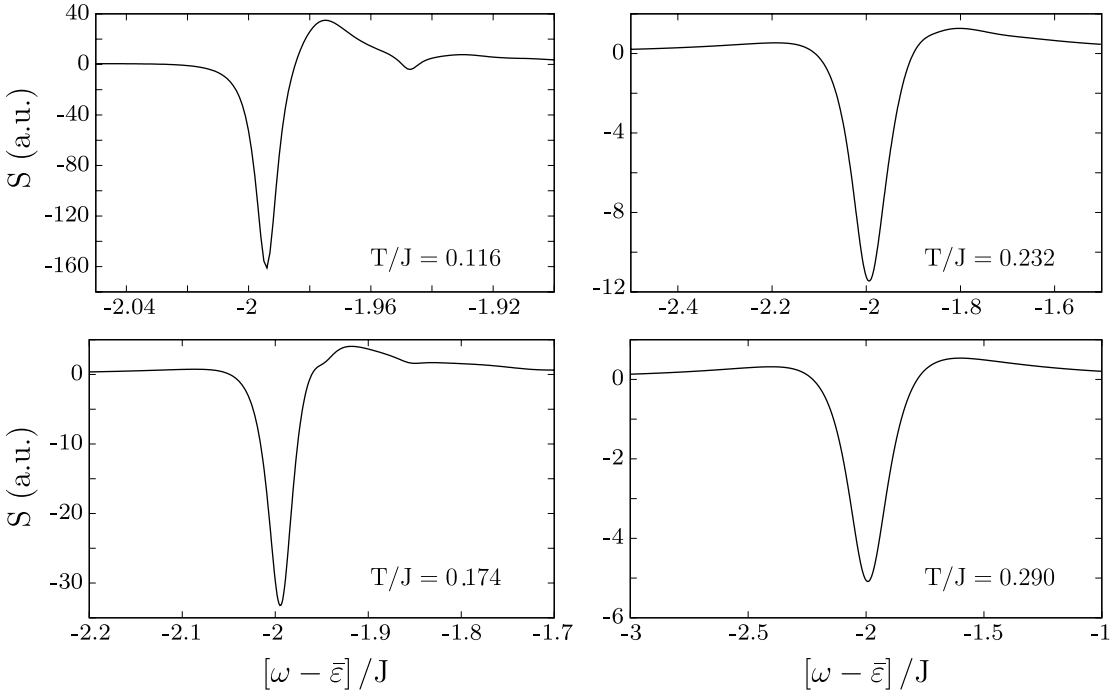

Fig. 5. Pump-probe spectra for $T/J = 0.116$ (top left), 0.174 (bottom left), 0.232 (top right), and 0.290 (bottom right) for a homogeneous chain with $N = 40$, taking $W_0/J = 25$. The pump-probe delay time τ was set to zero.

structure within localization segments, discussed in Section 4.2, and it has been proven numerically that, as long as the spectrum is dominated by inhomogeneous effects, indeed $\delta \sim 1/N_{\mathrm{del}}^2$ [16]. It was noted by Mukamel and coworkers, however, that at elevated temperatures δ should rather reflect the exciton coherence size as caused by scattering on vibrations [15]. Our current calculations, based on a microscopic picture of the exciton-vibration scattering rates, allow us to test this.

To perform such a test, we define a coherence length as obtained from the pump-probe spectrum through

$$N_{\mathrm{coh}}^{\mathrm{PP}}(T) = \sqrt{\frac{3\pi^2 J}{\delta(T)}}. \tag{13}$$

In Fig. 6 we plotted $1/N_{\mathrm{coh}}^{\mathrm{PP}}(T)$ against T for two aggregate sizes (symbols). The solid line represents the best power-law fit through the high-temperature points ($T > 0.12\,J$), where the coherence size does not depend on the chain length anymore (at low temperatures, the coherence length in our calculations is limited to the system size). The power-law fit reads

$$\frac{1}{N_{\mathrm{coh}}^{\mathrm{PP}}(T)} = 1.285(T/J)^{1.84}. \tag{14}$$

This scaling law may be compared with another one, found by defining the coherence length $N_{\mathrm{coh}}^{\Delta}(T)$ based on the temperature dependent width $\Delta(T)$ of the absorption band, leading to $1/N_{\mathrm{coh}}^{\Delta}(T) = b\sqrt{(\Delta(T) - \Delta(0))/2J}$, with b a constant of the order unity [27]. For homogeneous aggregates with nearest-neighbor interactions, $\Delta(T) - \Delta(0) = (W_0/2\pi J)\Gamma(\frac{7}{2})\zeta(\frac{7}{2})T^{7/2}$, with $\Gamma(z)$ and $\zeta(z)$ the Gamma and Riemann-zeta function, respectively [34]. For our current W_0 value, this leads to $1/N_{\mathrm{coh}}^{\Delta}(T) = 3.9b(T/J)^{7/4}$, which for $b \approx 0.33$ (i.e., in the order of unity) is in good agreement with the fit obtained above. This shows that, indeed, at elevated temperatures the pump-probe spectrum allows one to obtain the vibration-induced coherence length of the excitons.

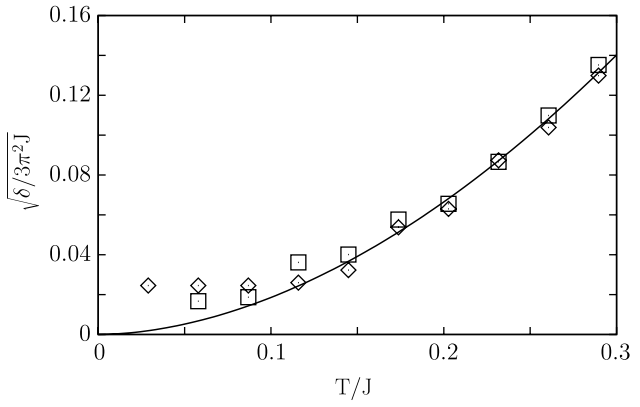

Fig. 6. Temperature dependence of $1/N_{\mathrm{coh}}^{\mathrm{PP}}$ (see Eq. (13)) for $N = 40$ (diamonds) and $N = 60$ (squares), taking $W_0/J = 25$. The solid curve indicates the powerlaw best fit through all high-temperature points.

6. Concluding remarks

In this paper, we have theoretically studied the pump-probe spectrum of linear molecular aggregates as measured through the use of ultrafast (femtosecond) pump and probe pulses. We have found that the shape of the spectrum is dominated by the well-known incoherent dispersive lineshape, arising from bleaching and stimulated emission contributions from the one-exciton band and blue-shifted induced-absorption contributions resulting from one- to two-exciton transitions. The blue-shift arises from the fermionic nature of the excitons in one dimension. The model predicts, however, that at low temperatures, where the linewidth is dominated by static disorder, also a small red-shifted induced-absorption peak occurs in the limit of small pump-probe delay time τ. This peak gets weaker for increasing disorder, but from our results it seems possible to observe it for commonly studied J-aggregates, such as PIC, where we expect the intensity of this new peak to be about 5–10% of the intensity of the main induced-absorption peak. It turns out that the peak can be associated with processes where the pump pulse generates a coherence between the first and third exciton state on a localization segment, which subsequently is promoted by the probe pulse to a state where both the first and second excited state of this segment are populated. As a function of τ, the coherent peak exhibits a decay due to inhomogeneous dephasing of many contributions with different oscillation frequencies, superimposed on an overall oscillation. Both the decay and the oscillation take place on a timescale proportional to the inverse zero-temperature linewidth $\Delta(0)$ of the absorption band (the J-band).

We have also considered the effects of thermal line broadening, resulting from homogeneous dephasing processes caused by scattering of the excitons on acoustic phonons in the aggregates' host medium. We have found that with increasing temperature the spectra tend to get more symmetric around the bleaching minimum, while the detuning δ between the bleaching peak and the blue-shifted induced-absorption maximum grows with temperature. The latter has indeed clearly been observed for the small B850 aggregates in the light-harvesting complex of purple bacteria [14] and for the cylindrical aggregates of amphiphilic cyanine dye molecules [18]. We have shown that δ provides a measure for the exciton coherence size induced by scattering on vibrations, similar to its use at low temperatures, where it measures the exciton delocalization size imposed by static disorder [16].

In this paper, we did not present results for the τ dependence of the pump-probe spectrum accounting for population redistribution and decay during the delay time (i.e., the effect of $\exp(\tilde{W}\tau)$ in Eq. (10) not being unity). We have calculated spectra taking such redistribution into account, but it turns out that the effects for common J-aggregates, such as PIC, are small and not particularly noteworthy.

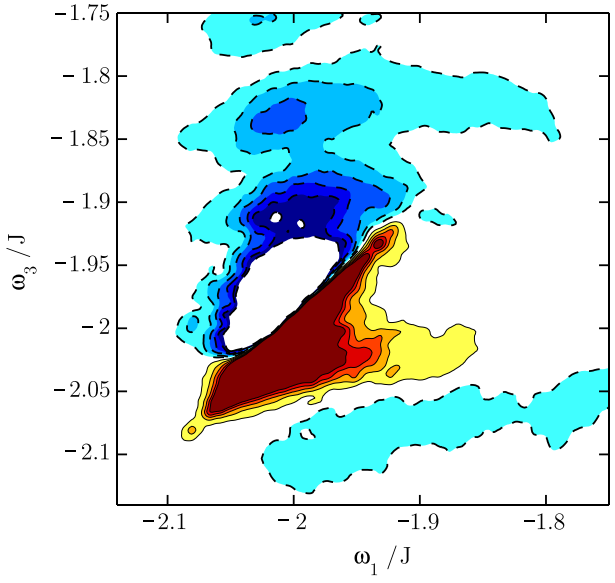

Fig. 7. Two-dimensional correlation spectrum for an aggregate with $N = 60$, $\sigma = 0.1J$ and a homogeneous line width $\gamma = 0.005J$. The waiting time τ is zero. Dashed red (negative) contours show bleaching and stimulated emission processes. Solid blue (positive) contours represent induced absorption. Contours were drawn at ±1%, ±2%, ±3%, ±4%, ±5% and at +0.2% of the amplitude of the spectrum. (For interpretation of the references in color in this figure legend, the reader is referred to the web version of this article.)

Finally, we briefly make a connection to two-dimensional electronic spectroscopy. Recently, it has been realized that this third-order optical technique, which bears some resemblance to pump-probe spectroscopy, offers great power to uncover details of the exciton dynamics in molecular aggregates [35,36]. We have calculated such spectra for our model of a linear aggregate. An example for aggregates of 60 molecules with $\sigma/J = 0.1$ and a constant homogeneous linewidth is shown in Fig. 7. In this spectrum, ω_1 (ω_3) may loosely be interpreted as the pump (probe) frequency. The negative diagonal ($\omega_1 = \omega_3$) peak represents the bleaching of the one-exciton band; the diagonal stretching derives from the inhomogeneous (static) nature of the line broadening (small homogeneous broadening). The induced absorption is clearly recognized as the positive peak that is blue-shifted in the ω_3 direction. Below the main diagonal, however, we also observe a weak positive peak. This is the analog of the coherent peak in our pump-probe spectra. We observe that in the two-dimensional spectrum the peak seems to form a low-frequency island, which may enhance the possibility to observe it. A more extensive study of the two-dimensional spectrum will be published elsewhere.

Acknowledgements

We thank Victor A. Malyshev for helpful discussions. Support from NanoNed, a national nanotechnology programme coordinated by the Dutch Ministry of Economic Affairs, is gratefully acknowledged.

Appendix

In this appendix, we present expressions for the various vibration-induced relaxation rates relevant to the calculation of the pump-probe signal. The method underlying the relaxation model used here is a second-order perturbation expansion in the exciton–phonon interaction Eq. (6) to obtain the evolution of the reduced density operator in the exciton subspace. As usual, we adhere to the Markov approximation. Hence, the rates may be calculated using the Fermi golden rule. The method has been explained in quite a number of text books and we refer to two good examples for the general formalism [37,38]. We note that in addition to the scattering on vibrations, we will also account for radiative decay. Then, the following quantities determine the relaxation processes.

First, the radiative decay rates of the one-exciton state k to the ground state, and of the two-exciton state $|K\rangle$ to one-exciton state $|k\rangle$, which read, respectively, $\gamma_{gk} = \gamma_0|\mu_{kg}|^2$ and $\gamma_{kK} = \gamma_0|\mu_{Kk}|^2$, with γ_0 the radiative constant of a single molecule.

Second, the scattering rates within the one- and two-exciton bands, induced by the one-phonon scattering interaction Eq. (6). These read

$$W_{kk'} = \sum_n \varphi_{kn}^2 \varphi_{k'n}^2 \mathscr{F}(|\omega_{kk'}|) G(\omega_{kk'}), \tag{15a}$$

for scattering from the one-exciton state k' to the state k (see Ref. [39] for a derivation) and (using a similar derivation)

$$W_{KK'} = \sum_{n>m} \sum_{n'>m'} (\delta_{nn'} + \delta_{nm'} + \delta_{mn'} + \delta_{mm'}) \times \varphi_{Knm}\varphi_{K'nm}\varphi_{Kn'm'}\varphi_{K'n'm'} \mathscr{F}(|\omega_{KK'}|) G(\omega_{KK'}), \tag{15b}$$

for scattering from the two-exciton state K' to the state K. Here, $\omega_{kk'} = E_k - E_{k'}$, $\omega_{KK'} = E_K - E_{K'}$, and $G(\omega) = \bar{n}(\omega)$ if $\omega > 0$ and $G(\omega) = \bar{n}(-\omega) + 1$ if $\omega < 0$, with $\bar{n}(\omega_q) = [\exp(\omega_q/T) - 1]^{-1}$ denoting the mean occupation of the phonon mode q at temperature T (we set the Boltzmann constant $k_B = 1$). Finally, the spectral density $\mathscr{F}(\omega)$ combines information of the density of states of the phonon bath with the energy dependence of the exciton phonon coupling (see definition in Eq. (7)).

All relevant population and coherence relaxation rates can now be expressed in terms of the above quantities. In particular, we obtain: (i) the homogeneous dephasing rate of the coherences $|k\rangle\langle g|$ and $|g\rangle\langle k|$ between the ground state and the one-exciton state k:

$$\Gamma_{kg} = \Gamma_{gk} = \frac{1}{2}\left[\gamma_{gk} + \sum_{k'} W_{k'k}\right]; \tag{16}$$

(ii) the homogeneous dephasing rate of the coherences $|k\rangle\langle k'|$ between any two different one-exciton states ($k \neq k'$):

$$\Gamma_{kk'} = \Gamma_{kg} + \Gamma_{k'g}; \tag{17}$$

(iii) the homogeneous dephasing rate of the coherences between a one-exciton state and a two-exciton state:

$$\Gamma_{Kk} = \Gamma_{kK} = \Gamma_{kg} + \frac{1}{2}\left[\sum_{k'} \gamma_{k'K} + \sum_{K'} W_{K'K}\right]; \tag{18}$$

(iv) the relaxation matrix for the one-exciton populations

$$\tilde{W}_{kk'} = -2\delta_{kk'}\Gamma_{kg} + (1-\delta_{kk'})W_{kk'}. \tag{19}$$

The latter matrix governs the Pauli master equation for the populations P_k in the one-exciton subspace

$$\dot{P}_k = \sum_{k'} \tilde{W}_{kk'} P_{k'}, \tag{20}$$

formally solved through

$$P_k(t) = \sum_{k'} \left[\mathrm{e}^{\tilde{W}\tau}\right]_{kk'} P_{k'}(t-\tau). \tag{21}$$

References

[1] E.E. Jelley, Nature 139 (1937) 631.
[2] G. Scheibe, Angew. Chem. 50 (1937) 212.
[3] J. Knoester, in: V.M. Agranovich, G.C. La Rocca (Eds.), Proceedings of the International School of Physics "Enrico Fermi, Course CXLIX", IOS Press, Amsterdam, 2002, p. 149.
[4] R. Gadonas, R. Danielus, R. Piskarskas, S. Rentsch, Izv. Akad. Nauk SSSR, Ser. Fiz. 47 (1983) 2445 [Bull. Acad. Sci. USSR, Phys. Ser. 47 (1983) 151].
[5] G. Juzeliūnas, Z. Phys. D 8 (1988) 379.
[6] H. Fidder, J. Knoester, D.A. Wiersma, J. Chem. Phys. 98 (1993) 6564.
[7] A.E. Johnson, S. Kumazaki, K. Yoshihara, Chem. Phys. Lett. 211 (1993) 511.
[8] K. Minoshima, M. Taiji, K. Misawa, T. Kobayashi, Chem. Phys. Lett. 218 (1994) 67.
[9] F.C. Spano, Chem. Phys. Lett. 220 (1994) 365.
[10] J.R. Durrant, J. Knoester, D.A. Wiersma, Chem. Phys. Lett. 222 (1994) 450.
[11] M. van Burgel, D.A. Wiersma, K. Duppen, J. Chem. Phys. 102 (1995) 20.
[12] J. Moll, S. Daehne, J.R. Durrant, D.A. Wiersma, J. Chem. Phys. 102 (1995) 6362.
[13] T. Pullerits, M. Chachisvilis, V. Sundström, J. Phys. Chem. 100 (1996) 10787.
[14] M. Chachisvilis, O. Kühn, T. Pullerits, V. Sundström, J. Phys. Chem. B 101 (1997) 7275.
[15] T. Meier, V. Chernyak, S. Mukamel, J. Phys. Chem. B 101 (1997) 7332.
[16] L.D. Bakalis, J. Knoester, J. Phys. Chem. B 103 (1999) 6620.
[17] M. Bednarz, J. Knoester, J. Phys. Chem. B 105 (2001) 12913.
[18] S.S. Lampoura, C. Spitz, S. Daehne, J. Knoester, K. Duppen, J. Phys. Chem. B 106 (2002) 3103.
[19] D.B. Chesnut, A. Suna, J. Chem. Phys. 39 (1963) 146.
[20] F.C. Spano, Phys. Rev. Lett. 67 (1991) 3424.
[21] L.A. Staehelin, J.R. Golecki, G. Drews, Biochim. Biophys. Acta 589 (1980) 30.
[22] A.R. Holzwarth, K. Schaffner, Photosynth. Res. 41 (1994) 225.
[23] G. McDermott, S.M. Prince, A.A. Freer, A.M. Hawthornthwaite-Lawless, M.Z. Papiz, R.J. Cogdell, N.W. Isaacs, Nature 374 (1995) 517.
[24] H. van Amerongen, L. Valkunas, R. van Grondelle, Photosynthetic Excitons, World Scientific, Singapore, 2000.
[25] S. Kirstein, H. von Berlepsch, C. Böttcher, C. Burger, A. Ouart, G. Reck, S. Daehne, ChemPhysChem 3 (2000) 146.
[26] M. Bednarz, V.A. Malyshev, J. Knoester, Phys. Rev. Lett. 91 (2003) 217401.
[27] D.J. Heijs, V.A. Malyshev, J. Knoester, Phys. Rev. Lett. 95 (2005) 117402.
[28] J. Knoester, Phys. Rev. A 47 (1993) 2083.
[29] S. Mukamel, Principles of Nonlinear Optical Spectroscopy, Oxford University Press, Oxford, 1995.
[30] A.V. Malyshev, V.A. Malyshev, Phys. Rev. B 63 (2001) 195111.
[31] M. Schreiber, Y. Toyozawa, J. Phys. Soc. Jpn. 51 (1982) 1528; M. Schreiber, Y. Toyozawa, J. Phys. Soc. Jpn. 51 (1982) 1537.
[32] A. Boukahil, D.L. Huber, J. Lumin. 45 (1990) 13.
[33] J. Köhler, A.M. Jayannavar, P. Reineker, Z. Phys. B 75 (1989) 451.
[34] D.J. Heijs, V.A. Malyshev, J. Knoester, J. Chem. Phys. 123 (2005) 144507.
[35] T. Brixner, J. Stenger, H.M. Vaswani, M. Cho, R.E. Blankenship, G.R. Fleming, Nature 434 (2005) 625.
[36] I. Stiopkin, T. Brixner, M. Yang, G.R. Fleming, J. Phys. Chem. B 110 (2006) 20032.
[37] K. Blum, Density Matrix Theory and Applications, second ed., Plenum Press, New York, 1996.
[38] V. May, O. Kühn, Charge and Energy Transfer Dynamics in Molecular Systems, Wiley-VCH, Berlin, 2000.
[39] M. Bednarz, V.A. Malyshev, J. Knoester, J. Chem. Phys. 117 (2002) 6200.